# Design criteria for scanning tunneling microscopes to reduce the response to external mechanical disturbances

Christian R. Ast,[1,a)] Maximilian Assig,[1] Alexandra Ast,[2] and Klaus Kern[1,3]
[1]*Max-Planck-Institut für Festkörperforschung, 70569 Stuttgart, Germany*
[2]*Institute of Engineering and Computational Mechanics, University of Stuttgart, 70569 Stuttgart, Germany*
[3]*Institut de Physique des Nanostructures, Ecole Polytechnique Fédérale de Lausanne (EPFL), CH-1015 Lausanne, Switzerland*

(Received 16 May 2008; accepted 17 August 2008; published online 26 September 2008)

We present a simple one-dimensional model to find design criteria for a scanning tunneling microscope (STM) minimizing the response of the tip-sample distance to external mechanical disturbances. The underlying concept—achieving a response that is in phase and same amplitude—goes beyond the conventional approach to construct the STM as stiff as possible. It introduces optimization conditions relating the resonance frequencies of the different components to the STM assembly, which can be implemented accordingly during the STM design process. In this way an improvement in the response to external disturbances of several orders of magnitude can be achieved. Calculations for three typical STM designs are presented along with the corresponding optimization criteria. For one of the designs an improvement in performance has been experimentally verified. The results can also be extended to other scanning probe techniques.  [DOI: 10.1063/1.2979008]

In a scanning tunneling microscope (STM), the tunneling current depends exponentially on the tip-sample distance,[1,2] which makes it an extremely sensitive experimental tool. During a topography scan the tip-sample distance is controlled such that the tunneling current remains constant. Therefore, it is necessary to minimize the effects of external mechanical disturbances inducing an unwanted background signal in the tunneling current since it is *a priori* impossible to distinguish it from the actual signal from the sample.[3] Care must be taken to isolate the measurement setup as effectively as possible from the surrounding environment. Different approaches are various active and/or passive damping stages on which the whole experimental setup is resting.[4–10] Others are to push the resonance frequencies as high as possible by building the STM as rigid as possible or to decouple the STM, e.g., by means of an eddy current damping stage.[11] These approaches work for most experimental setups quite successfully. However, under some conditions it is not possible or sufficient to apply the above damping mechanisms. For example, eddy current damping does not work if magnetic fields are to be applied, and external damping stages may be insufficient when operating a flow cryostat[12,13] or a dilution refrigerator because they present internal sources of mechanical noise, which are not adequately damped by external damping stages.

Here we present an approach to reduce the response of the tip-sample distance to disturbances, which induce an unwanted signal in the tunneling current. The idea is to optimize the design of the STM itself so that the response of the tip and the sample to disturbances is in phase and with same amplitude over a broad range of frequencies. In this way, the response of the tip-sample distance to disturbances can be significantly reduced. We present a simple one-dimensional model from which we derive a number of optimization criteria for different STM designs that are commonly in use. The results presented here for STMs can also be extended to other scanning probe techniques.

In the following, we will discuss three STM designs, which essentially only differ by how the coarse approach mechanism is implemented. Schematics of these designs are shown in the left panels of Fig. 1. For the modeling we only consider the immediate surroundings of the tip and the sample. All systems employ a coarse-motion mechanism (4) as well as a scan piezo (3), which moves the tip (2). They are connected to the rest of the experimental structure by a base plate (5) from which disturbances couple to the STM. The design in Fig. 1(a), which we have constructed, uses an attocube coarse-motion piezo stage.[14] However, in the calculation this coarse motor can also be substituted by a different coarse-motion mechanism, e.g., the "Pan-design."[15] The sample (1) is held by a cylindrical housing (6). The other designs shown in Figs. 1(b) and 1(c) are two "beetle-type" STMs,[16] which differ only in the locations of the scan piezo (3) and the sample (1). In this design the coarse-motion piezos (4) are mounted on the base plate (5). The ramp (7) holds the sample (1) or the scan piezo (3) in Fig. 1(b) or 1(c), respectively.

In order to formulate a simple mathematical model for these different STM designs, a few assumptions and simplifications have to be made. The simplified models are shown in the right panels of Fig. 1. They focus on the disturbances and the motion of the system to which the tip-sample distance is most sensitive. Therefore, these models are one dimensional and consider only the longitudinal motion of the flexible components while any bending motion is neglected. Since the bending motion has nonetheless some influence on

a)Author to whom correspondence should be addressed. Electronic mail: c.ast@fkf.mpg.de.

 

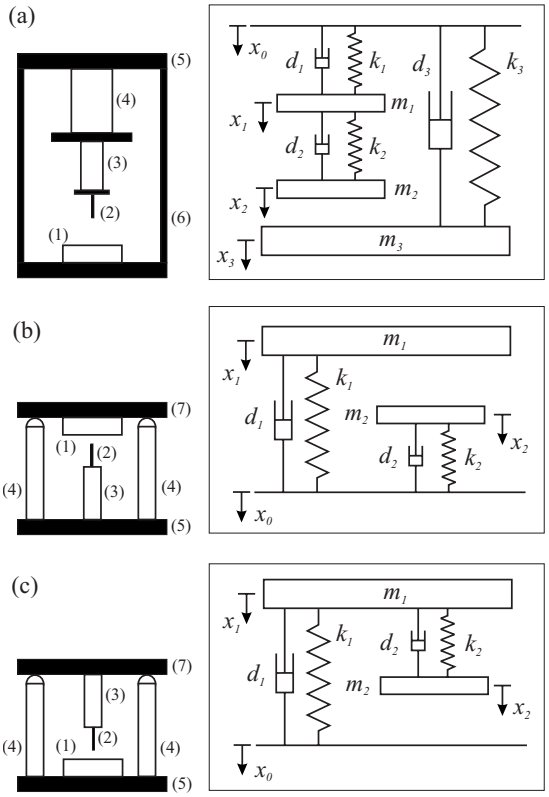


FIG. 1. Different design concepts for a STM: (a) Design using an attocube coarse motor (model 1), (b) beetle-type STM with a moving sample (model 2), and (c) beetle-type STM with a moving tip (model 3). (1) sample, (2) tip, (3) scan piezo, (4) coarse-motion piezo(s), (5) fixed mounting plate, (6) cylinder to hold the sample, and (7) ramp moving on top of the piezo-coarses.

the STM performance, it will be considered separately below. All piezos as well as the cylinder (6) in Fig. 1(a) are modeled as massless springs (spring constant $k_i$) with internal viscous damping $d_i$.[17] All other bodies (tip, sample, ramp, etc.) are assumed to be rigid bodies with mass $m_i$. Typical values for these quantities are given in Table I. The assumption to separate masses and spring constants is feasible because by design the different bodies are connected in series and the piezos are usually softer in relation to other parts of the construction.[17,18] To make the model more accurate, an effective mass of a part modeled as a spring can be attributed accordingly to the rigid bodies. The correspondence between the different masses and springs as well as the actual parts in the STM designs can be easily seen in Fig. 1.

To each mass $m_i$ a coordinate $x_i$ is assigned, which describes the deviation from the steady state position. The coordinate $x_0$ is associated with the disturbance, i.e., it models the motion of the base plate. The equations of motion[18] are

TABLE I. Typical values for the different masses $m_i$ (in g) and spring constants $k_i$ (in $N/\mu m$) in the different STM models. Models 1–3 refer to Figs. 1(a)–1(c), respectively.

| Model | $m_1$ | $m_2$ | $m_3$ | $k_1$ | $k_2$ | $k_3$ |
|---|---|---|---|---|---|---|
| 1 | 15 | 2 | 200 | 600 | 26.4 | 650 |
| 2 and 3 | 20 | 1.8 | n/a | 79.2 | 26.4 | n/a |
| 1 (opt) | 15 | 2 | 67.681 | 600 | 26.4 | 650 |

$$\boldsymbol{M}_j\ddot{\boldsymbol{x}} = \boldsymbol{K}_j\boldsymbol{x} + \boldsymbol{D}_j\dot{\boldsymbol{x}} + \boldsymbol{H}_j\ddot{x}_0. \tag{1}$$

The index $j$ refers to the models 1–3. The coordinates $x_i$ are combined in the displacement vector $\boldsymbol{x}=[x_0x_1x_2x_3]^T$. $\boldsymbol{M}_j$, $\boldsymbol{K}_j$, and $\boldsymbol{D}_j$ are the mass, stiffness, and damping matrices, respectively. The vector $\boldsymbol{H}_j$ is necessary to incorporate the second time derivative of the disturbance $\ddot{x}_0$ into the equation, which is comparable to a force exciting the system. The different matrices are

$$\boldsymbol{M}_1 = \begin{bmatrix} 1 & 0 & 0 & 0 \\ 0 & m_1 & 0 & 0 \\ 0 & 0 & m_2 & 0 \\ 0 & 0 & 0 & m_3 \end{bmatrix},$$

$$\boldsymbol{K}_1 = \begin{bmatrix} 0 & 0 & 0 & 0 \\ k_1 & -k_1-k_2 & k_2 & 0 \\ 0 & k_2 & -k_2 & 0 \\ k_3 & 0 & 0 & -k_3 \end{bmatrix},$$

$$\boldsymbol{D}_1 = \begin{bmatrix} 0 & 0 & 0 & 0 \\ d_1 & -d_1-d_2 & d_2 & 0 \\ 0 & d_2 & -d_2 & 0 \\ d_3 & 0 & 0 & -d_3 \end{bmatrix}, \quad \boldsymbol{H}_1 = \begin{bmatrix} 1 \\ 0 \\ 0 \\ 0 \end{bmatrix}, \tag{2}$$

$$\boldsymbol{M}_2 = \begin{bmatrix} 1 & 0 & 0 \\ 0 & m_1 & 0 \\ 0 & 0 & m_2 \end{bmatrix}, \quad \boldsymbol{K}_2 = \begin{bmatrix} 0 & 0 & 0 \\ k_1 & -k_1 & 0 \\ k_2 & 0 & -k_2 \end{bmatrix},$$

$$\boldsymbol{D}_2 = \begin{bmatrix} 0 & 0 & 0 \\ d_1 & -d_1 & 0 \\ d_2 & 0 & -d_2 \end{bmatrix}, \quad \boldsymbol{H}_2 = \begin{bmatrix} 1 \\ 0 \\ 0 \end{bmatrix}, \tag{3}$$

$$\boldsymbol{M}_3 = \begin{bmatrix} 1 & 0 & 0 \\ 0 & m_1 & 0 \\ 0 & 0 & m_2 \end{bmatrix}, \quad \boldsymbol{K}_3 = \begin{bmatrix} 0 & 0 & 0 \\ k_1 & -k_1-k_2 & k_2 \\ 0 & k_2 & -k_2 \end{bmatrix},$$

$$\boldsymbol{D}_3 = \begin{bmatrix} 0 & 0 & 0 \\ d_1 & -d_1-d_2 & d_2 \\ 0 & d_2 & -d_2 \end{bmatrix}, \quad \boldsymbol{H}_3 = \begin{bmatrix} 1 \\ 0 \\ 0 \end{bmatrix}. \tag{4}$$

Using the state vector $\boldsymbol{z}=[\boldsymbol{x}^T\dot{\boldsymbol{x}}^T]^T$ as well as the input variable $u=\ddot{x}_0$ and defining $y$ as the output variable, the equations of motion in state space form[19] can be written as

$$\dot{\boldsymbol{z}} = \boldsymbol{A}_j\boldsymbol{z} + \boldsymbol{B}_j u,$$

$$y = \boldsymbol{C}_j\boldsymbol{z}, \tag{5}$$

where the matrices $\boldsymbol{A}_j$, $\boldsymbol{B}_j$, and $\boldsymbol{C}_j$ are defined as

$$\boldsymbol{A}_j = \begin{bmatrix} 0 & \boldsymbol{E} \\ \boldsymbol{M}_j^{-1}\boldsymbol{K}_j & \boldsymbol{M}_j^{-1}\boldsymbol{D}_j \end{bmatrix},$$

$$\boldsymbol{B}_j = \begin{bmatrix} 0 \\ \boldsymbol{M}_j^{-1}\boldsymbol{H}_j \end{bmatrix},$$

$$\boldsymbol{C}_1 = \begin{bmatrix} 0 & 0 & 1 & -1 & 0 & 0 & 0 & 0 \end{bmatrix},$$

$$\boldsymbol{C}_2 = \begin{bmatrix} 0 & 1 & -1 & 0 & 0 & 0 \end{bmatrix},$$

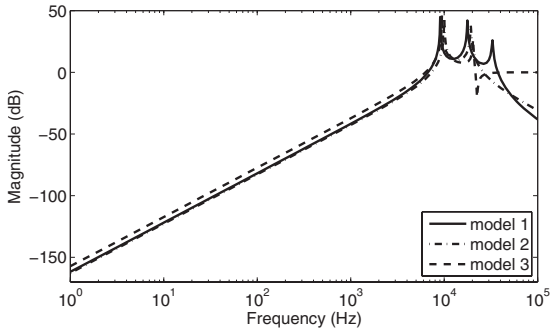


FIG. 2. Magnitude Bode plot for the transfer functions of the tip-sample distance in the design using an attocube coarse motor (model 1), the beetle-type STM with a moving sample (model 2), and the beetle-type STM with a moving tip (model 3). Typical values have been used for the design parameters.

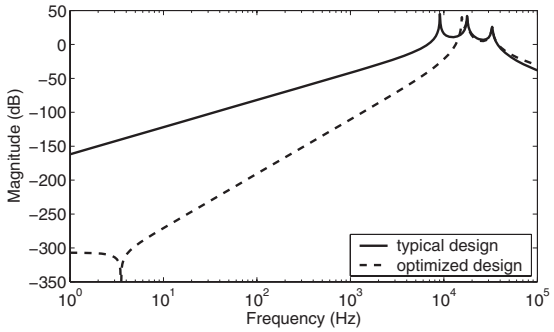


FIG. 3. Magnitude Bode plot for the typical and optimized transfer functions of the tip-sample distance in model 1. The values are given in Table I. The improvement can be several orders of magnitude.

$$\boldsymbol{C}_3 = \begin{bmatrix} 1 & 0 & -1 & 0 & 0 & 0 \end{bmatrix}. \tag{6}$$

The output matrices $\boldsymbol{C}_j$ are chosen such that the output variable $y$ yields the tip-sample distance. Taking the Laplace transform of Eq. (5) (the transformed variables are denoted by the corresponding capital letters), the corresponding transfer functions $G_j(s)$ can be obtained[19]

$$G_j(s) = \frac{Y(s)}{X_0(s)} = s^2 \boldsymbol{C}_j (s\boldsymbol{E} - \boldsymbol{A}_j)^{-1} \boldsymbol{B}_j. \tag{7}$$

The factor $s^2$ originates in the Laplace transform ($\ddot{x}_0 \mapsto s^2 X_0$) of the input variable.

The results are displayed for typical values of the masses and spring constants (see Table I) in a magnitude Bode plot in Fig. 2 for models 1–3. Some general features are the fairly high resonance frequencies in all three models. For excitation frequencies below the lowest resonance frequency, the response of the tip-sample distance decreases as the excitation frequency decreases. In this regime the individual transfer functions of tip and sample are close to one resulting in a value close to zero for the transfer function of the tip-sample distance, which shows that the response is almost in phase and with same amplitude. For excitation frequencies above the highest resonance frequency the values for the transfer functions decrease again for models 1 and 2. Here, the individual transfer functions approach zero resulting again in a value close to zero for the transfer function of the tip-sample distance. For model 3, however, the value approaches 1 (0 dB). This can be understood by seeing that the sample in this model is directly coupled to the base plate and, therefore, to the excitation. The response for the tip assembly, however, will decrease with increasing excitation frequency leaving the system with an oscillating sample.

The frequency range relevant to the performance of the STM lies well below the lowest resonance frequency shown in Fig. 2. At 80 Hz, for example, we find a value of about −84 dB, which means a reduction of about four orders of magnitude in relation to the excitation amplitude. This means that the excitation amplitude has to be smaller than 10 nm if the resulting oscillations of the tip-sample distance, i.e., the noise in the $z$-direction, should not exceed 1 pm.

To improve the performance, the objective is to minimize the response of the tip-sample distance to disturbances coupling to the base plate. The ideal case would be if the transfer function $G_i(s)$ were zero over the whole frequency range meaning no response to disturbances. This, however, even in the simple models presented here, is not always possible. The transfer functions for the different models are in analytical form

$$G_1(s) = \frac{1}{\frac{m_1 m_2}{k_1 k_2} s^4 + \left( \frac{m_2}{k_2} + \frac{m_1 + m_2}{k_1} \right) s^2 + 1} - \frac{1}{\frac{m_3}{k_3} s^2 + 1},$$

$$G_2(s) = \frac{1}{\frac{m_1}{k_1} s^2 + 1} - \frac{1}{\frac{m_2}{k_2} s^2 + 1},$$

$$G_3(s) = \frac{1}{\frac{m_1 m_2}{k_1 k_2} s^4 + \left( \frac{m_2}{k_2} + \frac{m_1 + m_2}{k_1} \right) s^2 + 1} - 1. \tag{8}$$

The damping values have been set to zero here and in the following since they are assumed to be small compared to the other quantities. The main result is not altered by this assumption. The optimization criteria [i.e., $G_i(s) = \min$] for each model become evident by comparing the coefficients in Eq. (8). For model 1 the highest order term $s^4$ can be neglected because in the low frequency range, which is of interest here, it is small compared to the other terms. For models 1 and 2 the conditions are

$$\text{Model 1:} \frac{m_3}{k_3} = \frac{m_2}{k_2} + \frac{m_1 + m_2}{k_1},$$

$$\text{Model 2:} \frac{m_1}{k_1} = \frac{m_2}{k_2}. \tag{9}$$

For model 3 no optimization condition can be found. The only way to improve the performance of this type of STM would be to build it as stiff and light as possible to push the resonance frequencies as high as possible. This is not necessary for the other two models because in these cases an optimization means a matching of resonance frequencies. For model 2 the transfer function actually becomes identically zero. This represents the ideal case. For model 1 this yields a minimum in response, which is displayed in Fig. 3 for the values given in Table I [see model 1 (opt)]. The mass $m_3$ has been adjusted to meet the optimization criterion in Eq. (9). A general improvement in the response in the lower frequency range for the optimized response (dashed line) compared to the response for the "typical" values (solid line)

can be observed. At 80 Hz, for example, the optimized response now shows a reduction of −198.6 dB, which is an improvement by almost six orders of magnitude. In this case a 1 pm noise level can theoretically be achieved already for disturbances less than 1 mm.

Even though the models used here are quite simple, they do show whether or not it is in principle possible to improve the performance of a particular STM design. Applying these concepts to a real system, the response will only yield an estimate of the actual performance since other resonances from, e.g., bending motion, which generally lie lower in frequency than for the longitudinal motion, can interfere with the performance of the STM. This is because not only the vertical tip-sample distance is important but also a steady horizontal position of the tip with respect to the sample. Nevertheless, the optimization conditions in Eq. (9) give excellent criteria for improving the performance of a particular STM design.

For a real system, it is much more practical to determine the transfer function of a STM design from a set of resonance frequencies obtained from a computer aided design (CAD) model by the finite element method (FEM) (Ref. 20) than to assign the appropriate masses and spring constants. Therefore, the transfer functions need to be rewritten in terms of the model's resonance frequencies $\omega_i$

$$G_1(s) = \frac{1}{\left(\frac{s^2}{\omega_1^2}+1\right)\left(\frac{s^2}{\omega_2^2}+1\right)} - \frac{1}{\frac{s^2}{\omega_3^2}+1},$$

$$G_2(s) = \frac{1}{\frac{s^2}{\omega_1^2}+1} - \frac{1}{\frac{s^2}{\omega_2^2}+1},$$

$$G_3(s) = \frac{1}{\left(\frac{s^2}{\omega_1^2}+1\right)\left(\frac{s^2}{\omega_2^2}+1\right)} - 1. \tag{10}$$

It should be noted that the resonance frequency $\omega_i$ is not equal to $\sqrt{k_i/m_i}$ for the coupled oscillators. The optimization conditions in terms of the resonance frequencies are

$$\text{Model } 1: \omega_3^2 = \frac{\omega_1^2\omega_2^2}{\omega_1^2+\omega_2^2},$$

$$\text{Model } 2: \omega_1 = \omega_2. \tag{11}$$

The lowest resonance frequencies of the longitudinal motion obtained by a modal analysis of the finite-element model of the STMs can then be used to determine the individual $\omega_i$. For model 1, the design of the coarse approach mechanism as well as the scan piezo with the tip will be fairly set in most cases. Therefore, the minimized response could be realized by matching the resonance frequency $\omega_3$ of the outer cylinder to the optimization condition. For model 2, probably a combination of design changes for the scan piezo with the tip, the ramp with the sample as well as the coarse-motion piezos is necessary to fulfill the optimization condition in Eq. (11).

In order to test these design criteria, we have optimized a STM design that was built according to model 1. A sectional drawing of the original and new STM designs used in the experiments is shown in Figs. 4(a) and 4(b), respectively. For clarity, unnecessary details have been omitted and only the outlines of the piezos are shown. The coarse-motion piezo is a commercial $z$-stage by attocube.[14] The scan piezo is a lead zirkonate titanate (PZT) ceramic tube and the outer cylinder is made of copper. While the original design employs a cylindrical fixture to hold the sample, in the new design this has been changed to a conical shape with different inner and outer slopes in order to increase its resonance frequency.

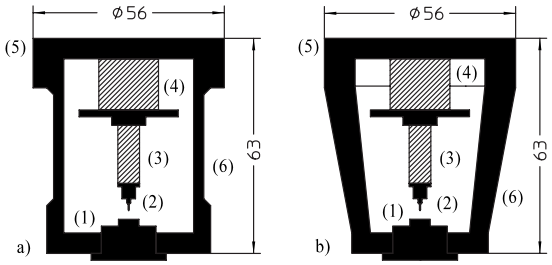


FIG. 4. (a) Original design and (b) new design of the STM that has been used in the experiments. (1) sample, (2) tip, (3) scan piezo, (4) coarse-motion piezo(s), (5) fixed mounting plate, and (6) cylinder/cone to hold the sample. All dimensions are given in millimeter.

The resonance frequencies for the coupled oscillators (coarse motion and scan piezos) have been determined by a FEM simulation from a CAD model ($\omega_1 = 15.467$ kHz and $\omega_2 = 23.681$ kHz). The resonance frequency of the original design for the outer cylinder was $\omega_3 = 7.683$ kHz and for the optimized design it would be $\omega_3^{\text{opt}} = 12.949$ kHz. The magnitude of the transfer functions for the different designs is shown in Fig. 5. In the low frequency range, the transfer function of the optimized design (dashed-dotted line) yields an improvement of about six orders of magnitude compared to the original design (solid line). The actual new design (dashed line) represents a compromise to accommodate spacial constraints in the design such as some space for the bias voltage contact on the sample. The resulting resonance frequency for this new design according to the FEM simulation was $\omega_3^{\text{new}} = 11.572$ kHz. In order to achieve this, the cylinder holding the sample has been changed to a more conical shape. The resulting improvement in response compared to the original design is about one order of magnitude. This is also already a substantial improvement and it can enhance the performance of the STM.

It is difficult to experimentally verify the improvement in the performance of the STM after the optimization proce-

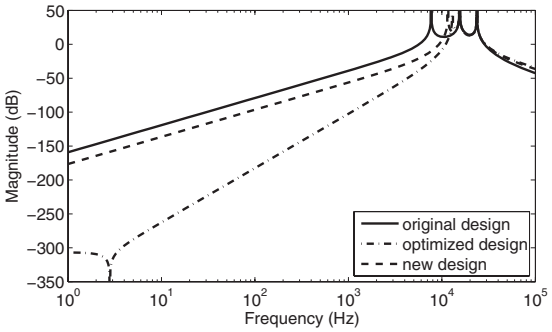


FIG. 5. Magnitude Bode plot for the original, optimized, and new STM designs.

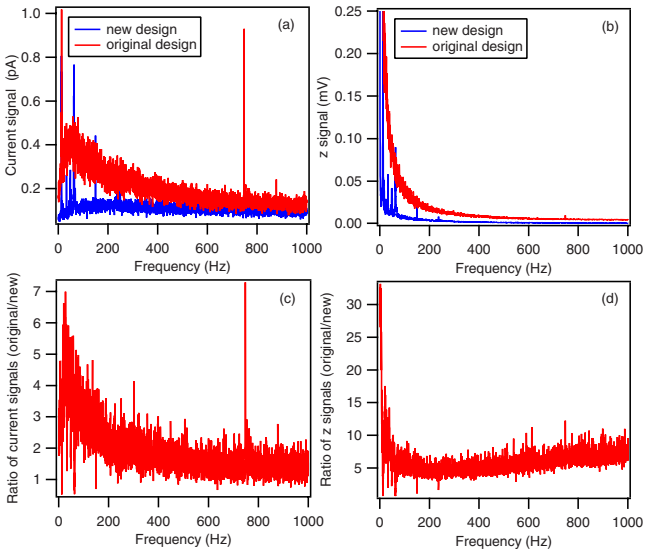


FIG. 6. (Color online) Fourier transforms of the (a) tunneling current and the (b) $z$-signal before (red/light gray) and after (blue/dark gray) the design optimization. The ratio between the original and new designs is shown for the tunneling current in (c) and for the $z$-signal in (d).

dure. This is essentially because the tunneling junction between tip and sample strongly depends on the quality of the tip and the sample, which makes it difficult to reproduce the same conditions for the measurements before and after the design optimization. Nevertheless, we have used both the original and new designs for an extended period of time to monitor the performance under different tunneling junctions. The graphs in Figs. 6(a) and 6(b) show the Fourier transforms of the tunneling current and the $z$-piezosignal measured over time when the tip is resting and the feedback loop is closed. They represent the best results for the STM design before and after the optimization. The red (light gray) and blue (dark gray) curves correspond to the original and the new designs, respectively. The measurements were done at room temperature on a clean Ag(111) surface. The tunneling current was $I=0.1$ nA with a bias voltage of $U_B=1$ V. The feedback loop parameters were also the same for both configurations. Both the current signal and the $z$-piezosignal clearly show a reduction in amplitude over the whole frequency range. In addition, the noise in the spectrum is also reduced for the new design compared to the original design.

In order to quantify the improvement in the response in the new design, the ratios between the original and new designs for the current signal and the $z$-piezosignal are plotted in Figs. 6(c) and 6(d), respectively. For the current signal there is an improvement by a factor between 2 and 5 for frequencies lower than 200 Hz. Above 200 Hz the factor lies between 1.5 and 2. For the $z$-piezosignal the improvement is always better than a factor of 5 and in the low frequency range it increases up to a factor of about 14. Overall this represents a significant improvement in the performance of the STM. In the real system other kinds of motion such as bending motion contribute to the response of the tip-sample distance to disturbances. As these and other effects have not been considered in our simple one-dimensional model, the improvement in performance is reduced compared to the theoretically predicted value.

The dynamics of the bending motion can be analyzed independently of the longitudinal motion since only small flexible deformations occur here and the motions are therefore decoupled.[21] Nevertheless, an optimization of the resonance frequencies of the longitudinal motion affects the bending motion as well because both resonance frequencies of bending and longitudinal motions are a function of the complex geometry of the STM. Thus, a simultaneous optimization of bending and longitudinal motions becomes very complicated, if possible at all.

Similar to the approach for the longitudinal motion a transfer function of the form

$$G_B(s) = \frac{1}{\frac{s^2}{\omega_{1B}^2} + 1} - \frac{1}{\frac{s^2}{\omega_{2B}^2} + 1} \tag{12}$$

can be derived for bending motions in model 1,[21] which relates horizontal disturbances in one direction acting at the base plate to horizontal deviations in the same direction of the tip from the sample. The index $B$ denotes the bending motion. Since the STM is rotationally symmetric, the same dynamics applies to the bending motion in the perpendicular horizontal direction. A reduction in response to the bending motion, i.e., by matching the frequencies $\omega_{1B}$ and $\omega_{2B}$ in Eq. (12), contributes thus more to the stability of the position of the tip rather than to the actual tip-sample distance, which is another important criterion in the performance of the STM. The optimization condition for the bending motion is similar to the optimization condition for $G_2$ in Eqs. (10) and (11).

In order to check if by optimizing the longitudinal dynamics the bending motion has been negatively affected, the lowest resonance frequencies of the bending motion of the tip assembly and the sample have been calculated for the new STM design (model 1) by FEM modal analysis as before for the longitudinal motion. The tip assembly (coarse motor, scan piezo, and tip) has a bending resonance at $\omega_{1B}=2.01$ kHz. This remained untouched by the optimization process. The bending resonance for the original design for the sample (outer cylinder and sample) was at $\omega_{2B}=1.76$ kHz while for the new design it was at $\omega_{2B}^{\text{new}}=2.386$ kHz. As noted above, it is extremely difficult to satisfy both optimization criteria for the bending motion and for the longitudinal motion at the same time. Nevertheless, the bending resonances in the new design are positioned such that the response is effectively the same. However, it should be noted that further extending the attocube coarse-motion piezo[14] results in a slightly lower bending resonance, which in turn results in a slightly worse response in the bending motion for the new design.

In conclusion, we have presented a simple one-dimensional model to calculate the response of the tip-sample distance in a STM to disturbances. We have shown that it is possible to significantly reduce this response by demanding that the tip and the sample react with the same amplitude and phase. The transfer functions for three different STM designs have been derived to find straightforward optimization conditions for design improvements. While for design 1 and design 2 an optimization condition could be found (for design 2 the transfer function actually becomes zero), the only possibility to optimize design 3 is to build the

components as stiff as possible. Using FEM analysis to find the corresponding resonance frequencies the optimization criteria can be directly incorporated into the design process of a new STM. The experimental implementation demonstrated that even though a very simple approach for the derivation of the optimization conditions was used, a noticeable improvement in performance is achievable in the actual STM as well.

We gratefully acknowledge fruitful discussions with W. Stiepany. C.R.A. acknowledges funding from the Emmy-Noether-Program of the Deutsche Forschungsgemeinschaft (DFG).

[1] G. Binning, H. Rohrer, Ch. Gerber, and E. Weibel, Appl. Phys. Lett. **40**, 178 (1982).
[2] G. Binning, H. Rohrer, Ch. Gerber, and E. Weibel, Phys. Rev. Lett. **49**, 57 (1982).
[3] External vibrations can only be identified in topographic scans as they appear mirrored in the forward and backward scans.
[4] D. W. Pohl, IBM J. Res. Dev. **30**, 417 (1986).
[5] M. Okano, K. Kajimura, S. Wakiyama, F. Sakai, W. Mizutani, and M. Ono, J. Vac. Sci. Technol. A **5**, 3313 (1987).
[6] A. I. Oliva, M. Aguilar, and V. Sosa, Meas. Sci. Technol. **9**, 383 (1998).
[7] P. Krapf, J. P. Lainé, Y. Robach, and L. Porte, J. Phys. III **5**, 1871 (1995).
[8] M. J. Rost, L. Crama, P. Schakel, E. van Tol, G. B. E. M. van Velzen-Williams, C. F. Overgauw, H. ter Horst, H. Dekker, B. Okhuijsen, M. Seynen, A. Vijftigschild, P. Han, A. J. Katan, K. Schoots, R. Schumm, W. van Loo, T. H. Oosterkamp, and J. W. M. Frenken, Rev. Sci. Instrum. **76**, 053710 (2005).
[9] D. Croft and S. Devasia, Rev. Sci. Instrum. **70**, 4600 (1999).
[10] C. J. Chen, *Introduction to Scanning Tunneling Microscopy* (Oxford University Press, New York, 1993).
[11] S. Park and C. F. Quate, Rev. Sci. Instrum. **58**, 2004 (1987).
[12] S. Behler, M. K. Rose, J. C. Dunphy, D. F. Ogletree, M. Salmeron, and C. Chapeller, Rev. Sci. Instrum. **68**, 2479 (1997).
[13] M. Bott, T. Michely, and G. Comsa, Rev. Sci. Instrum. **66**, 4135 (1995).
[14] Model: ANPz50/LT/UHV z-positioner, http://www.attocube.de
[15] S. H. Pan, E. W. Hudson, and J. C. Davis, Rev. Sci. Instrum. **70**, 1459 (1999).
[16] K. Besocke, Surf. Sci. **181**, 145 (1987).
[17] D. J. Inman, *Engineering Vibration* (Prentice-Hall, Englewood Cliffs, 1994).
[18] R. C. Hibbeler, *Engineering Mechanics—Dynamics* (Prentice-Hall, Upper Saddle River, 2006).
[19] R. C. Dorf and R. H. Bishop, *Modern Control Systems* (Prentice-Hall, Upper Saddle River, 2001).
[20] K. J. Bathe, *Finite Element Procedures* (Prentice-Hall, Upper Saddle River, 1996).
[21] P. Hagedorn and A. Das Gupta, *Vibration and Waves in Continous Mechanical Systems* (Wiley, Chichester, 2007).